Shape, shell structure, and low-lying strong octupole strength in $^{60}_{20}Ca_{40}$

I. Hamamoto,[1] H. Sagawa,[2] and X. Z. Zhang[1,3]
[1]*Department of Mathematical Physics, Lund Institute of Technology at University of Lund, Lund, Sweden*
[2]*Center for Mathematical Sciences, University of Aizu, Ikki-machi, Aizu-Wakamatsu, Fukushima 965, Japan*
[3]*Institute of Atomic Energy, Beijing, People's Republic of China*
(Received 20 February 2001; published 11 July 2001)

Properties of the possible *l-s* closed shell nucleus $^{60}_{20}Ca_{40}$, which is expected to be spherical in the ground state, are studied, using the self-consistent Hartree-Fock calculation plus the random-phase approximation with Skyrme interactions. The possible disappearance of the magic number $N=50$ is suggested in nuclei near the neutron drip line. In particular, the low-lying octupole threshold strength, which may be strongly collective due to the disappearance of the $N=50$ magic number, is pointed out.

DOI: 10.1103/PhysRevC.64.024313 PACS number(s): 21.60.Jz, 21.10.Pc, 23.20.Js, 27.50.+e

I. INTRODUCTION

The study of the properties of nuclei far from the β stability line is one of the most exciting research fields in nuclear physics. The shell structure and magic numbers can be drastically changed near neutron drip lines. For example, in the neutron drip line of very light nuclei it has been observed that $N=20$ [1] and $N=8$ [2] are no longer magic numbers, while $N=16$ may be a new magic number [3]. In Ref. [4] the basic elements playing an important role in changing the shell structure in the neighborhood of the neutron drip line are studied. Since the neutron drip line for $Z \lesssim 28$ will be within reach with the new experimental facilities, which will come into use in several years, more information on the change of the shell structure in nuclei in the vicinity of the neutron drip line with $N \lesssim 60$ will become available in the near future.

Extrapolating the binding-energy systematics of known Ca isotopes, the nucleus $^{60}_{20}Ca_{40}$ is expected to lie just inside the neutron drip line and can be reached experimentally. As $^{80}_{40}Zr_{40}$ is known most probably to be deformed, $^{60}_{20}Ca_{40}$ could be the heaviest (spherical) *l-s* closed shell nucleus, in which low-lying collective 2^+ states are absent. In Ref. [5] the quadrupole strength function and the resulting electric polarization charge of $^{60}_{20}Ca_{40}$ were studied. Though the low-lying quadrupole threshold strength is obtained in the nucleus, the threshold strength is dominated by the unperturbed neutron strength. If there are no low-lying 0^+ states, which are either deformed or two-particle-two-hole $(2p\text{-}2h)$ or $4p\text{-}4h$ states, the lowest excited state will have negative parity. Then, there is a good chance to observe collective octupole strength as low-lying threshold strength. Using the self-consistent Hartree-Fock (HF) plus the random-phase approximation (RPA) with Skyrme interactions, we study the properties of $^{60}_{20}Ca_{40}$, taking into account simultaneously both the isoscalar (IS) and isovector (IV) correlation. The RPA equation is solved in coordinate space with Green's function method so that the states in the continuum are properly estimated.

In Sec. II the shape and shell structure of $^{60}_{20}Ca_{40}$ are studied. Furthermore, the dependence of the possible magic number $N=50$ (and the one-particle energy gap at $N=40$) on the proton number is investigated. In Sec. III the octupole response function of $^{60}_{20}Ca_{40}$ is estimated. In Sec. IV the discussion and conclusion are given.

II. SHAPE AND SHELL STRUCTURE

The lowest excited 2^+ state in $^{80}_{40}Zr_{40}$ is observed at Ex $=290$ keV [6] and, thus, the nucleus must be deformed, though there has been no direct evidence for the shape of the deformation. In another $N=40$ nucleus, $^{68}_{28}Ni_{40}$, the lowest excited state is found to be $I^\pi=0^+$ at Ex$=1.77$ MeV [7] while the second excited state is 2^+ at Ex$=$ 2.03 MeV [8]. The $B(E2;0^+\rightarrow 2^+)$ value has recently been measured [9] to be about 3.5 W.u., which indicates the rigidity against quadrupole deformation of the nucleus. The energy of the 2^+_1 state in $^{68}_{28}Ni_{40}$ is determined approximately by the energy of the lowest-lying proton *p-h* excitation $1f_{7/2}\rightarrow 2p_{3/2}$. The lowest-lying negative-parity state of $^{68}_{28}Ni_{40}$ is the 5^- state observed [10] at Ex$=2.85$ MeV, and no 3^- state has so far been identified.

First, we estimate the HF total energy of $N=40$ nuclei as a function of quadrupole deformation to explore the stiffness of the spherical shape. In Fig. 1 the total energy estimated with a constrained HF calculation and the SIII interaction is shown for $^{60}_{20}Ca_{40}$ and $^{68}_{28}Ni_{40}$ as a function of the quadrupole moment. In order to obtain a convergence in the constrained HF calculation, the pair correlation parameter $\Delta_n=\Delta_p$ $=0.7$ MeV was introduced in the numerical calculations. The spherical HF minimum of $^{60}_{20}Ca_{40}$ can be easily obtained without introducing any pair-correlation parameters, and the calculated minimum energy is almost equal to the value plotted in Fig. 1(a). Calculations with Skyrme interactions other than the SIII interaction produce very similar results. In $^{60}_{20}Ca_{40}$ we find no local energy minimum other than the one at $Q=0$ (namely, spherical shape) and the calculated energy increases steeply for nonzero values of Q. The *l-s* closed shell nucleus is seen to be very rigid against quadrupole deformation. In contrast, in $^{68}_{28}Ni_{40}$ we obtain a shallow local energy minimum for a prolately deformed shape, which may correspond to the observed 0^+ state at Ex$=1.77$ MeV. The same type of calculations for $^{80}_{40}Zr_{40}$ is known to exhibit at least three local energy minima for the oblate, spherical, and prolate shapes. For example, see Ref. [11].

The nucleus $^{60}_{20}Ca_{40}$ has a large neutron excess and, thus, the calculated root-mean-square value of neutrons at the

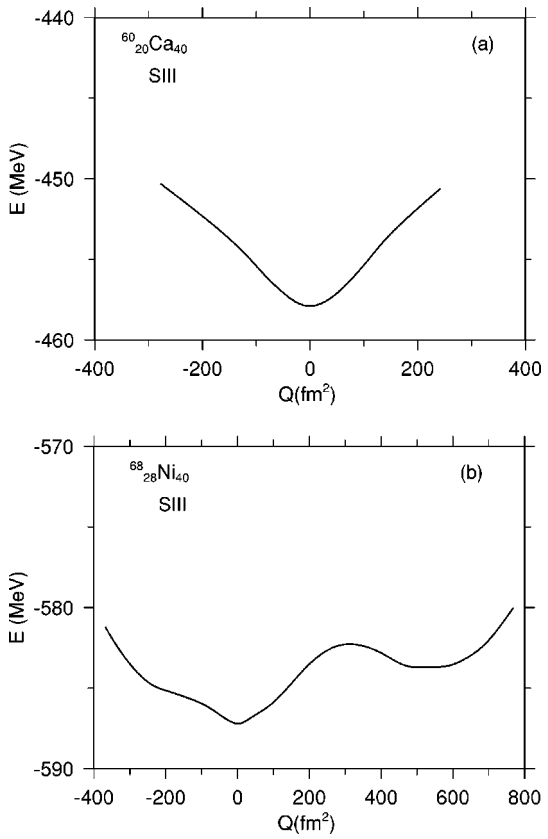

FIG. 1. The total energy as a function of the calculated quadrupole moment, obtained by constrained HF calculations. The SIII interaction is used. (a) $^{60}_{20}Ca_{40}$; (b) $^{68}_{28}Ni_{40}$.

spherical HF minimum is about 10% larger than that of protons: $\sqrt{\langle r_n^2\rangle}$ and $\sqrt{\langle r_p^2\rangle}$ are 4.033 and 3.625 fm for the SIII interaction, while 4.085 and 3.614 fm for the SkM* interaction, respectively.

In Fig. 2 we show the single-particle energy levels together with the HF potentials of $^{60}_{20}Ca_{40}$, $^{68}_{28}Ni_{40}$, and $^{80}_{40}Zr_{40}$, which are calculated using a spherical HF code with the SkM* interaction. For $^{60}_{20}Ca_{40}$ we show also the figure calculated with the SIII interaction, for reference. We note that $Z=50$ is always a good magic number, namely, the energy distance between two proton levels $2d_{5/2}$ and $1g_{9/2}$, is considerable for all three nuclei $^{80}_{40}Zr_{40}$, $^{68}_{28}Ni_{40}$, and $^{60}_{20}Ca_{40}$. In contrast, $N=50$ seems to be a good magic number in $^{80}_{40}Zr_{40}$ and $^{68}_{28}Ni_{40}$, while the magic number may be washed out in the neutron drip line nucleus $^{60}_{20}Ca_{40}$. Indeed, in $^{60}_{20}Ca_{40}$ the energy distance between the $1g_{9/2}$ neutron level and the $2d_{5/2}$ one-neutron resonant level is only 1.97 MeV in the HF calculation using the SkM* interaction and, moreover, the virtual $3s_{1/2}$ level is located below the $2d_{5/2}$ resonant level in the continuum [see Sec. III and Fig. 4(b)]. Since the $2d_{5/2}$ neutron level is not obtained as the one-particle resonant state for the HF potential with the SIII interaction, the energy gap at $N=50$ cannot be estimated in this case. The underlying cause of $2d$ levels becoming lower relative to $1g$ levels for very small binding energies of neutrons is mainly the smaller kinetic energies for orbits with smaller l values [4]. The calculated energy gap at $N=40$ is nearly the same for all three nuclei shown. Since the parity of one-particle levels above $N=40$ is different from the one below, the possible melting of the magic number $N=50$ does not directly lead to a quadrupole softness of $^{60}_{20}Ca_{40}$. On the other hand, the melting can be seen by the low-lying strong octupole strength. In contrast, in $^{68}_{28}Ni_{40}$ the low-lying collective octupole strength is not expected, since the lowest octupole excitation of proton *p-h* configurations is as high as 10 MeV due to the filling of the $1f_{7/2}$ shell and since the considerable size of the $N=50$ energy gap further prevents collective octupole strength from appearing at very low energy.

According to our experience in very light nuclei, HF calculations with available Skyrme interactions are known to produce too many nuclei lying inside the neutron drip line. For example, though both $^{28}_{8}O_{20}$ and $^{26}_{8}O_{18}$ are experimentally known to lie outside the neutron drip line, almost all HF calculations available predict these nuclei to be stable against neutron emission. Thus, one may say that the $1g_{9/2}$ neutron level should have been in the continuum of $^{60}_{20}Ca_{40}$, though it is obtained as a bound level in our calculation. This is because $^{70}_{20}Ca_{50}$ lies definitely inside the neutron drip line if the $1g_{9/2}$ level is bound already for $^{60}_{20}Ca_{40}$, and we know that the systematics of the measured neutron separation energy indicates $^{60}_{20}Ca_{40}$ to be already close to the neutron drip line. If the $1g_{9/2}$ neutron level is unbound, there may be no bound excited states and a stronger octupole strength may appear as threshold strength. The lowest-lying negative-parity state of $^{60}_{20}Ca_{40}$ may happen to be a 5^- state. However, the high-multipole state is very unlikely to be a collective state.

III. OCTUPOLE RESPONSE FUNCTION

The octupole response function of $^{60}_{20}Ca_{40}$ is studied by using the self-consistent HF calculation plus RPA with Skyrme interactions performed in coordinate space, which has previously been applied to monopole [12], dipole [13], quadrupole [5], and spin-dependent excitation modes [14]. A particularly interesting issue in this nucleus is that the lowest excited states would be negative-parity states and the low-lying octupole strength would be strongly collective.

We study the RPA response function

$$S(E)\equiv\sum_n |\langle n|O|0\rangle|^2\delta(E-E_n)=\frac{1}{\pi}\mathrm{Im\ Tr}[O^\dagger G_{\mathrm{RPA}}(E)O], \tag{1}$$

where O expresses the one-body operators

$$O_\mu^{\lambda=3,\,\tau=0}=\sum_i r_i^3 Y_{3\mu}(\hat{r}_i) \quad \text{for isoscalar octupole strength,} \tag{2}$$

$$O_\mu^{\lambda=3,\,\tau=1}=\sum_i \tau_z(i) r_i^3 Y_{3\mu}(\hat{r}_i)$$

$$\text{for isovector octupole strength.} \tag{3}$$

Taking the result calculated with the SkM* interaction, we explain the octupole response functions of $^{60}_{20}Ca_{40}$. As seen in Fig. 2(a), the calculated threshold energy is 3.41

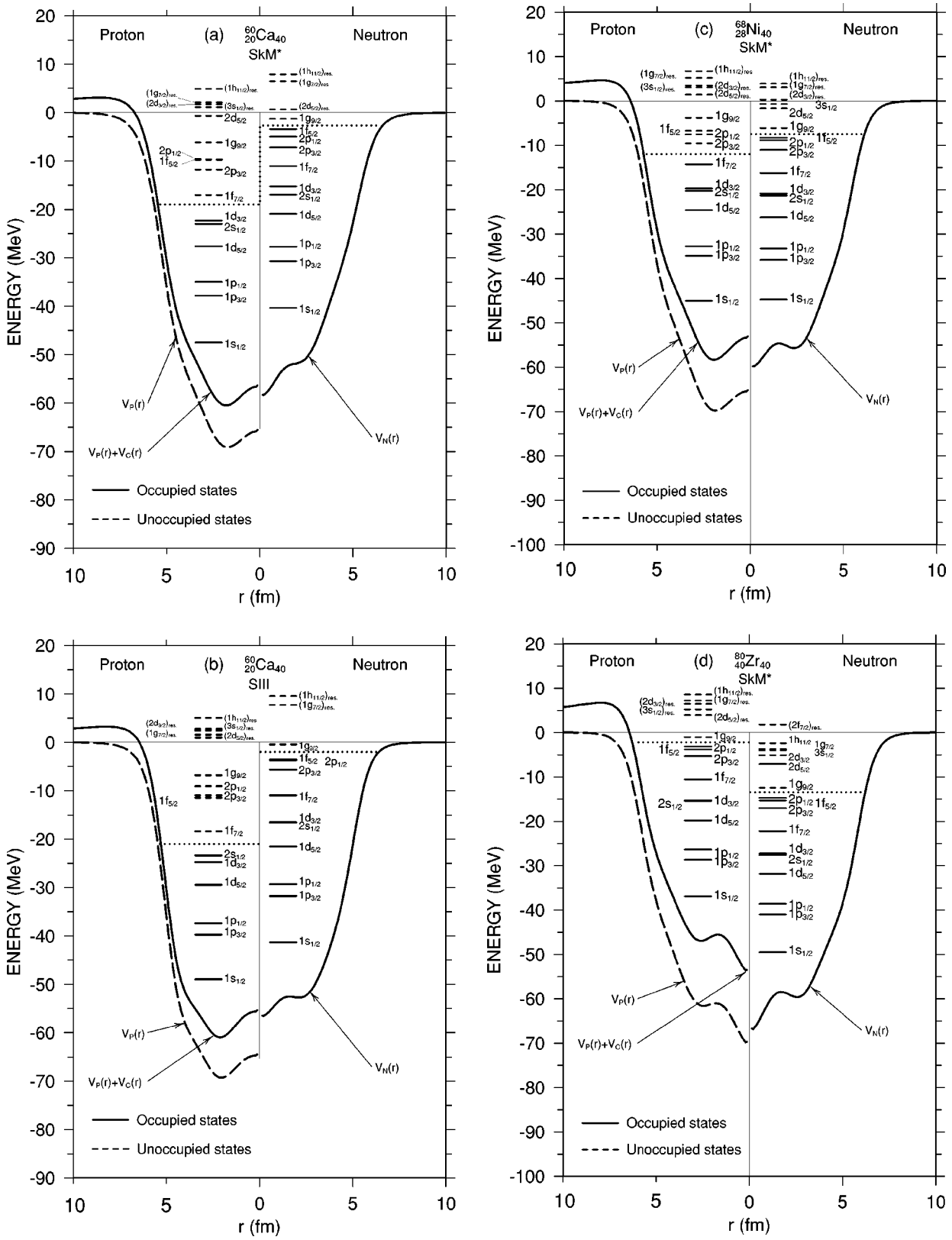

FIG. 2. Hartree-Fock potentials and one-particle energy levels. Neutrons on the right-hand side and protons on the left-hand side. $V_N(r)$ expresses the neutron nuclear potential, while $V_P(r)$ and $V_C(r)$ denote the proton nuclear and Coulomb potential, respectively. The notation $(nl_j)_{\mathrm{res}}$ expresses the calculated one-particle resonant levels in the HF potential. Occupied levels are indicated by full lines, while unoccupied levels are denoted by broken lines. The dotted line shows an approximate position of the Fermi level. (a) $^{60}_{20}Ca_{40}$ with the SkM* interaction; (b) $^{60}_{20}Ca_{40}$ with the SIII interaction; (c) $^{68}_{28}Ni_{40}$ with the SkM* interaction; (d) $^{80}_{40}Zr_{40}$ with the SkM* interaction.

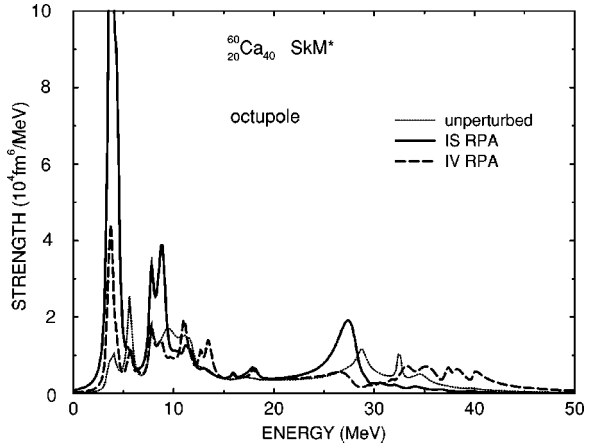

FIG. 3. Calculated octupole strengths $(gr,0^+\rightarrow 3^-)$ of the IS RPA, IV RPA, and unperturbed excitations to the continuum in $^{60}_{20}Ca_{40}$, which are shown by the solid, dashed, and dotted curves, respectively. The calculated strengths are folded with the width of 0.4 MeV to make the feature of the strength distribution easily recognizable. The SkM* interaction is used for both the HF and RPA calculation.

MeV, which is equal to the binding energy of the $1f_{5/2}$ neutrons. In the calculation the unoccupied $1g_{9/2}$ neutron orbital is predicted to be bound, though experimentally the orbital will most likely be in the continuum. Accepting this possible overbinding result, we proceed to study the octupole response functions.

In Fig. 3 the calculated strengths of the IS RPA, IV RPA, and unperturbed excitations to the continuum are shown. In order to make the feature of the strength distribution easily recognizable, the averaged strengths, which are folded with the width of 0.4 MeV, are shown. So-called $\Delta N=3$ giant octupole resonance (GOR) is identified as peaks around 26–28 and 33–40 MeV for the IS and IV strength, respectively. On the other hand, the $\Delta N=1$ IS GOR is, roughly speaking, divided into two parts; the major part of the strength is estimated to lie in the region of Ex$<$5 MeV, though an appreciable amount of the strength is located also at 7.5$\lesssim$Ex$\lesssim$9 MeV. Below the threshold at 3.41 MeV one RPA state is obtained at Ex=1.92 MeV with the calculated value of $B(E3{:}0^+\rightarrow 3^-)=2.31\times 10^3\ e^2$ fm^6 and $B(\lambda=3,IS{:}0^+\rightarrow 3^-)=3.78\times 10^4$ fm^6. The strongly collective IS peaks below 5 MeV are always seen to be accompanied by weaker peaks of the IV strengths, because in the collective IS oscillation the tendency to preserve the local ratio of neutrons and protons gives rise to an IV moment proportional to the neutron excess [15–17].

Since we are interested in the collectivity of lower-lying excitations, in Fig. 4(a) both the calculated strength of the IS RPA and that of unperturbed neutron excitations to the continuum are shown for Ex$<$12 MeV on an enlarged scale, while the unperturbed strengths obtained by exciting neutrons from each occupied orbital to the continuum are shown in Fig. 4(b). No folding procedure is carried out in Fig. 4, in contrast to Fig. 3. The strength summed over all unperturbed neutron strengths in Fig. 4(b) is plotted as the dotted curve in Fig. 4(a). The unperturbed excitations from bound to bound states in the region of Ex$<$9 MeV, which do not appear in

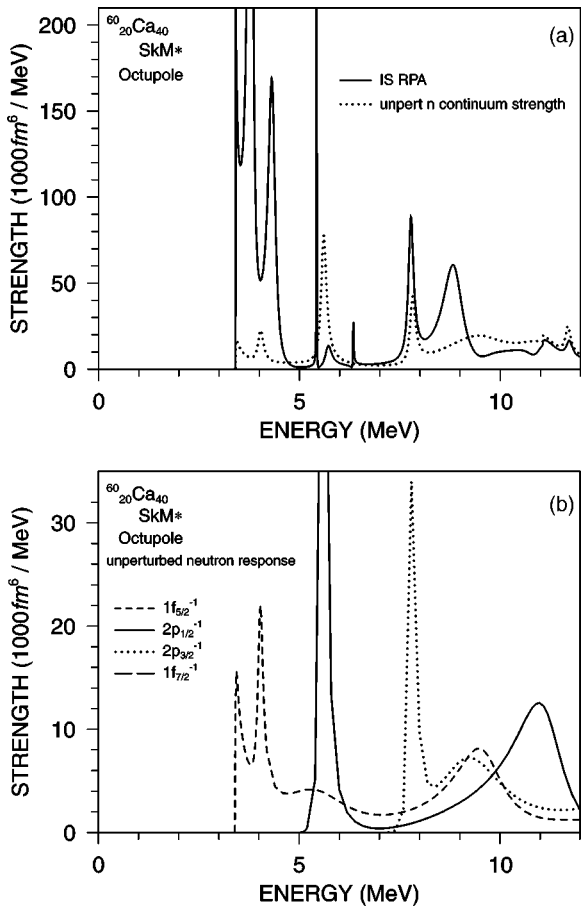

FIG. 4. Comparison of the low-lying octupole strength $(gr,0^+\rightarrow 3^-)$ of the IS RPA with that of the unperturbed neutron excitation to the continuum. The SkM* interaction is used. (a) The strength of IS RPA is shown by the solid curve, while the total strength of the unperturbed neutron excitation to the continuum is denoted by the dotted curve. (b) Unperturbed strength obtained by exciting neutrons from occupied orbitals to the continuum. See the text for details.

Fig. 4(b), are two neutron excitations, $1f_{5/2}\rightarrow 1g_{9/2}$ at 2.08 MeV and $2p_{3/2}\rightarrow 1g_{9/2}$ at 5.87 MeV, and two proton excitations, $1d_{3/2}\rightarrow 1f_{7/2}$ at 5.27 MeV and $2s_{1/2}\rightarrow 1f_{7/2}$ at 5.97 MeV. The contributions by these four unperturbed excitation strengths are not included in the dotted curve in Fig. 4(a). However, they appear naturally in the RPA strength due to the coupling to the continuum states. From Fig. 4(a) it is fairly clear that three peaks of the IS RPA strength at Ex $<$5 MeV originate from the three peaks of the dotted curve at 3.44, 4.04, and 5.61 MeV. The downward shifting of the peak energies is due to the attractive nature of the IS RPA correlation. The IS octupole strength of both higher-lying unperturbed peaks and the bound-to-bound excitations of protons and neutrons is strongly absorbed by the bound RPA state at 1.92 MeV and the three peaks at Ex$<$5 MeV. The presence of considerable contributions to these three peaks by proton excitations can be clearly seen in Fig. 3 by the large difference between the peak strengths of IS RPA and IV RPA.

The interpretation of the peaks in Fig. 4(b) can be made in the following way, examining the one-particle levels in Fig.

TABLE I. Energy weighted sum rule values of RPA IS octupole strength in $^{60}_{20}Ca_{40}$ and $^{68}_{28}Ni_{40}$ (expressed in %) calculated with SkM* and SIII interactions.

Energy interval (MeV)	$^{60}_{20}Ca_{40}$ (SkM*)	$^{60}_{20}Ca_{40}$ (SIII)	$^{68}_{28}Ni_{40}$ (SkM*)	$^{68}_{28}Ni_{40}$ (SIII)
0−5	14.6	14.3	7.0	6.1
5−10	13.4	18.5	13.4	19.2
10−15	8.9	7.1	9.3	4.2
15−20	8.1	6.8	6.0	8.9
20−30	41.5	38.3	47.3	45.0
30−40	8.4	11.6	9.2	10.1
40−60	1.7	2.2	2.5	2.7

2(a). For the excitation of neutrons in the $1f_{5/2}$ orbital indicated by the dashed curve, the lowest peak at 3.45 MeV comes from the $l=0$ threshold strength (or possibly the excitation to the virtual $3s_{1/2}$ state), while the peaks around 4.04, 5.3, and 9.5 MeV come from the excitations to the one-particle resonant $2d_{5/2}$ state, to the broad distribution of the virtual $2d_{3/2}$ state and to the one-particle resonant $1g_{7/2}$ state, respectively. For the excitation of neutrons in the $2p_{1/2}$ orbital shown by the solid curve, the excitations to the $l=0$ states as well as the virtual $2d_{3/2}$ state are absent, while the peaks around 5.6 and 11.0 MeV come from the excitations to the one-particle-resonant $2d_{5/2}$ and $1g_{7/2}$ states, respectively. In this way it is understood that the low energies of the unperturbed neutron excitations to the continuum are created by the disappearance of the $N=50$ magic number. If the energy distance between the $1g_{9/2}$ and $(2d_{5/2})_{\rm res}$ levels (or the virtual $3s_{1/2}$ level) were much larger, say 5 MeV, the peaks of the dotted curves in Fig. 4(a) would have been pushed up by 3 MeV.

In Table I we compare the calculated energy-weighted sum rule (EWSR) for the IS octupole strength of $^{60}_{20}Ca_{40}$ with those of $^{68}_{28}Ni_{40}$. It is seen that in the region of Ex <5 MeV in $^{60}_{20}Ca_{40}$ we obtain about 14% of the EWSR value of the IS octupole strength, compared with 6−7 % in the case of $^{68}_{28}Ni_{40}$. The higher-lying IS GOR in the region of Ex=25–30 MeV exhausts about 40% of EWSR in $^{60}_{20}Ca_{40}$, while about 46% of EWSR is exhausted in $^{68}_{28}Ni_{40}$. The low-lying extra strength in $^{60}_{20}Ca_{40}$ is, in essence, shifted from the higher-lying IS GOR. A shift of this amount is common in the results obtained by using the SIII and SkM* interaction.

IV. DISCUSSION AND CONCLUSION

The nucleus $^{60}_{20}Ca_{40}$ is predicted to be spherical and rigid against quadrupole deformation. Consequently, the lowest-lying excited states will have negative parity. If there are no discrete excited states, the low-lying excitation spectrum will be dominated by the collective octupole strength, which is strengthened by the possible disappearance of the traditional magic number $N=50$. The low-lying strong octupole strength should be detected also by a large renormalization of the one-particle octupole moment (namely, the polarization of the core) in the neighboring nuclei.

We have shown that the melting of the $N=50$ magic number can occur already in the absence of the possible pair correlation, as in the case of the $N=8$ and 20 magic numbers in very light nuclei close to the neutron drip line [4]. The rigid nature of $^{60}_{20}Ca_{40}$ against quadrupole deformation is hardly changed by the possible pair correlation, because of the one-particle shell structure in the *l-s* closed shell nucleus.

The calculated energy of the lowest 3^- state is governed by the energy of the unperturbed neutron *p-h* excitation, $1f_{5/2}\rightarrow 1g_{9/2}$. Thus, the calculated energy depends somewhat on the Skyrme interactions used. For examples, it is 2.56 MeV for the SIII interaction, while the SkM* interaction gives 1.92 MeV. However, the appearance of the strongly collective IS octupole strength in the low-energy region is commonly obtained in the calculations with Skyrme interactions.

ACKNOWLEDGMENTS

Two of the authors (I.H. and H.S.) are thankful to RIKEN, where we began the present work, for support. I.H. is grateful to Prof. M. Ishihara for his warm encouragement. The third author (X.Z.Z.) acknowledges the financial support provided by Crafoordska Stiftelsen, which makes it possible for him to work at the Lund Institute of Technology. H.S. acknowledges financial support by the Japanese Ministry of Education, Science, Sports and Culture by Grant-In-Aid for Scientific Research under Program No. C(2) 12640284. The authors express their thanks to Karin Ryde for a careful reading of the manuscript.

[1] D. Guillemaud-Mueller *et al.*, Nucl. Phys. **A426**, 37 (1984); T. Motobayashi *et al.*, Phys. Lett. B **346**, 9 (1995).
[2] H. Iwasaki *et al.*, Phys. Lett. B **481**, 7 (2000); H. Iwasaki *et al.*, *ibid.* **491**, 8 (2000).
[3] A. Ozawa, T. Kobayashi, T. Suzuki, K. Yoshida, and I. Tanihata, Phys. Rev. Lett. **84**, 5493 (2000).
[4] I. Hamamoto, S. Lukyanov, and X. Z. Zhang, Nucl. Phys. **A683**, 255 (2001).
[5] I. Hamamoto, H. Sagawa, and X. Z. Zhang, Nucl. Phys. **A626**, 669 (1997).
[6] C. J. Lister *et al.*, Phys. Rev. Lett. **59**, 1270 (1987).
[7] M. Bernas *et al.*, Phys. Lett. **113B**, 279 (1982).
[8] R. Broda *et al.*, Phys. Rev. Lett. **74**, 868 (1995).
[9] O. Sorlin *et al.*, Nucl. Phys. **A685**, 186c (2001); (to be published).
[10] T. Ishii, M. Asai, A. Makishima, I. Hossain, M. Ogawa, J. Hasegawa, M. Matsuda, and S. Oshikawa, Phys. Rev. Lett. **84**, 39 (2000).
[11] P. Bonche, H. Flocard, P. H. Heenen, S. J. Krieger, and M. S. Weiss, Nucl. Phys. **A443**, 39 (1985).
[12] I. Hamamoto, H. Sagawa, and X. Z. Zhang, Phys. Rev. C **56**, 3121 (1997).

[13] I. Hamamoto, H. Sagawa, and X. Z. Zhang, Phys. Rev. C **57**, R1064 (1998).
[14] I. Hamamoto and H. Sagawa, Phys. Rev. C **60**, 064314 (1999).
[15] A. Bohr and B. R. Mottelson, *Nuclear Structure* (Benjamin, Reading, MA, 1975), Vol. II, Chap. 6.
[16] I. Hamamoto, H. Sagawa, and X. Z. Zhang, Phys. Rev. C **55**, 2361 (1997).
[17] I. Hamamoto, Phys. Rev. C **60**, 031303(R) (1999).